where Λ_B is the value taken by Λ_o [equation (5.1.3.8)] in the Bragg case.

There is no longer a total-reflection domain but the extinction effect still exists, as is shown by the hyperbolic cosine term. The maximum height of the rocking curve decreases as the thickness of the crystal decreases.

(ii) $|\eta| > 1$:

$$I_h = \frac{1 - \cos^2[\pi(t/\Lambda_B)(\eta^2-1)^{1/2}]}{\eta^2 - \cos^2[\pi(t/\Lambda_B)(\eta^2-1)^{1/2}]},$$
$$I_o = \frac{\eta^2 - 1}{\eta^2 - \cos^2[\pi(t/\Lambda_B)(\eta^2-1)^{1/2}]}. \quad (5.1.7.7b)$$

The cosine terms show that the two wavefields propagating within the crystal interfere, giving rise to *Pendellösung* fringes in the rocking curve. These fringes were observed for the first time by Batterman & Hildebrandt (1967, 1968). The angular positions of the minima of the reflected beam are given by

$$\eta = \mp(K^2\Lambda_B^2 t^{-2} + 1)^{1/2},$$

where K is an integer.

Integrated intensity. The integrated intensity is

$$I_{hi} = \pi\delta \tanh[\pi t/\Lambda_B], \quad (5.1.7.8)$$

where t is the crystal thickness. When this thickness becomes very large, the integrated intensity tends towards

$$I_{hi} = \pi\delta. \quad (5.1.7.9)$$

This expression differs from (5.1.7.3) by the factor π, which appears here in place of 8/3. von Laue (1960) pointed out that because of the differences between the two expressions for the reflecting power, (5.1.7.2) and (5.1.7.7*b*), perfect agreement could not be expected. Since some absorption is always present, expression (5.1.7.3), which includes the factor 8/3, should be used for very thick crystals. In the presence of absorption, however, expression (5.1.7.8) for the reflected intensity for thin crystals does tend towards that for thick crystals as the crystal thickness increases.

Comparison with geometrical theory. When t/Λ_B is very small (thin crystals or weak reflections), (5.1.7.8) tends towards

$$I_{hi} = R^2\lambda^2 t|F_h|^2 \big/ (V^2\gamma_o \sin 2\theta), \quad (5.1.7.10)$$

which is the expression given by geometrical theory. If we call this intensity I_{hi}(geom.), comparison of expressions (5.1.7.8) and (5.1.7.10) shows that the integrated intensity for crystals of intermediate thickness can be written

$$I_{hi} = I_{hi}(\text{geom.})\frac{\tanh(\pi t/\Lambda_B)}{(\pi t/\Lambda_B)}, \quad (5.1.7.11)$$

which is the expression given by Darwin (1922) for primary extinction.

5.1.7.2.2. Absorbing crystals

Reflected intensity. The intensity of the reflected wave for a thin absorbing crystal is

$$I_h = |\gamma|\left|\frac{D_h^{(a)}}{D_o^{(a)}}\right|^2 = \left|\frac{F_h}{F_{\bar{h}}}\right| \frac{\cosh 2b - \cos 2a}{L\cosh 2b + (L^2-1)^{1/2}\sinh 2b - \cos(2a + 2\Psi')}, \quad (5.1.7.12)$$

where

$$2a = [\pi t/\Lambda_B]\rho\cos(\beta+\omega),$$
$$2b = [\pi t/\Lambda_B]\rho\sin(\beta+\omega).$$

L, ρ and ψ' are defined in (5.1.7.5), β is defined in (5.1.3.7) and ω is the phase angle of $(\eta^2-1)^{1/2}$.

Comparison with geometrical theory. When t/Λ_B decreases towards zero, expression (5.1.7.12) tends towards $[\sin(\pi t\eta/\Lambda_B)/\eta]^2$; using (5.1.3.5) and (5.1.3.8), it can be shown that expression (5.1.7.12) can be written, in the non-absorbing symmetric case, as

$$I_h = \frac{R^2\lambda^2C^2|F_h|^2t^2}{V^2\sin^2\theta}\left\{\frac{\sin[2\pi k\cos(\theta)t\Delta\theta]}{[2\pi k\cos(\theta)t\Delta\theta]}\right\}^2, \quad (5.1.7.13)$$

where d is the lattice spacing and $\Delta\theta$ is the difference between the angle of incidence and the middle of the reflection domain. This expression is the classical expression given by geometrical theory [see, for instance, James (1950)].

5.1.8. Real waves

5.1.8.1. Introduction

The preceding sections have dealt with the diffraction of a plane wave by a semi-infinite perfect crystal. This situation is actually never encountered in practice, although with various devices, in particular using synchrotron radiation, it is possible to produce highly collimated monochromated waves which behave like pseudo plane waves. The wave from an X-ray tube is best represented by a spherical wave. The first experimental proof of this fact is due to Kato & Lang (1959) in the transmission case. Kato extended the dynamical theory to spherical waves for non-absorbing (Kato, 1961*a*,*b*) and absorbing crystals (Kato, 1968*a*,*b*). He expanded the incident spherical wave into plane waves by a Fourier transform, applied plane-wave dynamical theory to each of these components and took the Fourier transform of the result again in order to obtain the final solution. Another method for treating the problem was used by Takagi (1962, 1969), who solved the propagation equation in a medium where the lateral extension of the incident wave is limited and where the wave amplitudes depend on the lateral coordinates. He showed that in this case the set of fundamental linear equations (5.1.2.20) should be replaced by a set of partial differential equations. This treatment can be applied equally well to a perfect or to an imperfect crystal. In the case of a perfect crystal, Takagi showed that these equations have an analytical solution that is identical with Kato's result. Uragami (1969, 1970) observed the spherical wave in the Bragg (reflection) case, interpreting the observed intensity distribution using Takagi's theory. Saka *et al.* (1973) subsequently extended Kato's theory to the Bragg case.

Without using any mathematical treatment, it is possible to make some elementary remarks by considering the fact that the divergence of the incident beam falling on the crystal from the source is much larger than the angular width of the reflection domain. Fig. 5.1.8.1(*a*) shows a spatially collimated beam falling

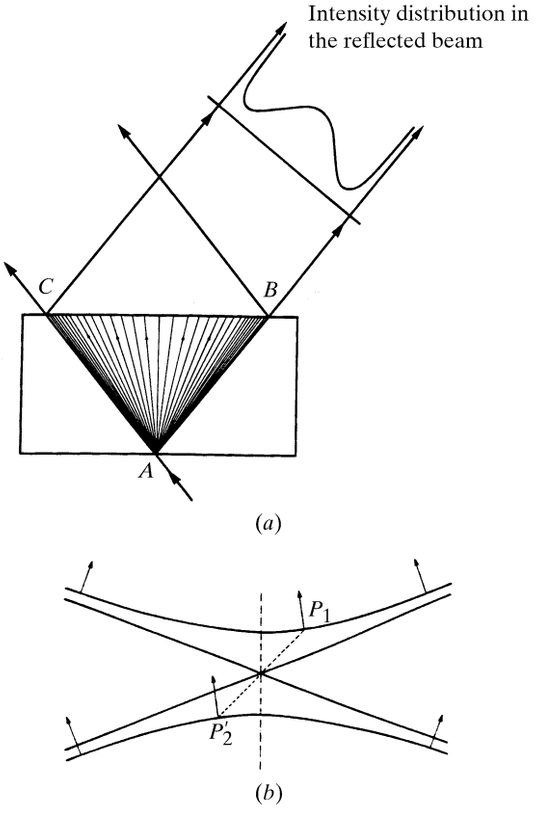

Fig. 5.1.8.1. Borrmann triangle. When the incident beam is divergent, the whole dispersion surface is excited and the wavefields excited inside the crystal propagate within a triangle filling all the space between the incident direction, AC, and the reflected direction, AB. Along any direction Ap within this triangle two wavefields propagate, having as tie points two conjugate points, P and P', at the extremities of a diameter of the dispersion surface. (*a*) Direct space; (*b*) reciprocal space.

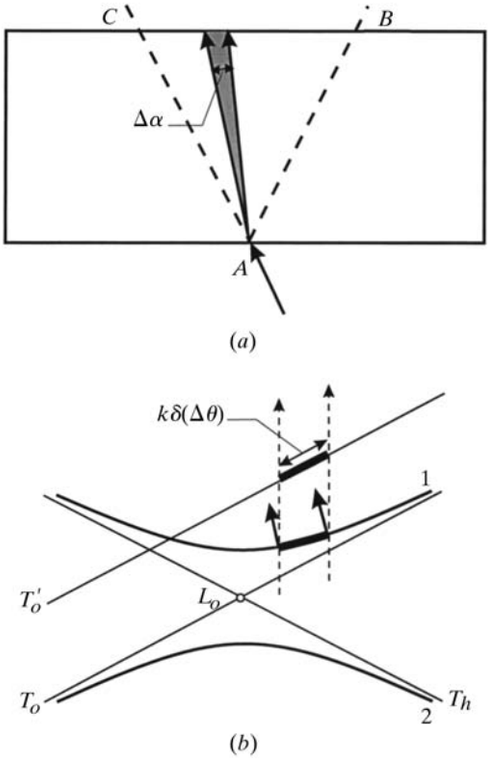

Fig. 5.1.8.2. Packet of wavefields of divergence $\Delta\alpha$ excited in the crystal by an incident wavepacket of angular width $\delta(\Delta\theta)$. (*a*) Direct space; (*b*) reciprocal space.

on a crystal in the transmission case and Fig. 5.1.8.1(*b*) represents the corresponding situation in reciprocal space. Since the divergence of the incident beam is larger than the angular width of the dispersion surface, the plane waves of its Fourier expansion will excite every point of both branches of the dispersion surface. The propagation directions of the corresponding wavefields will cover the angular range between those of the incident and reflected beams (Fig. 5.1.8.1*a*) and fill what is called the *Borrmann triangle*. The intensity distribution within this triangle has interesting properties, as described in the next two sections.

5.1.8.2. Borrmann triangle

The first property of the Borrmann triangle is that the angular density of the wavefield paths is inversely proportional to the curvature of the dispersion surface around their tie points. Let us consider an incident wavepacket of angular width $\delta(\Delta\theta)$. It will generate a packet of wavefields propagating within the Borrmann triangle. The angular width $\Delta\alpha$ (Fig. 5.1.8.2) between the paths of the corresponding wavefields is related to the radius of curvature $\mathcal{R}$ of the dispersion surface by

$$\mathcal{A} = \Delta\alpha/\delta(\Delta\theta) = k\cos\theta(\mathcal{R}\cos\alpha), \qquad (5.1.8.1)$$

where α is the angle between the wavefield path and the lattice planes [equation (5.1.2.26)] and $\mathcal{A}$ is called the amplification ratio. In the middle of the reflecting domain, the radius of curvature of the dispersion surface is very much shorter than its value, k, far from it (about 10^4 times shorter) and the amplification ratio is therefore very large. As a consequence, the energy of a wavepacket of width $\delta(\Delta\theta)$ in reciprocal space is spread in direct space over an angle $\Delta\alpha$ given by (5.1.8.1). The intensity distribution on the exit surface BC (Fig. 5.1.8.1*a*) is therefore proportional to $I_h/\mathcal{A}$. It is represented in Fig. 5.1.8.3 for several values of the absorption coefficient:

(i) Small values of $\mu_o t$ (less than 2 or 3) (Fig. 5.1.8.3*a*). The intensity distribution presents a wide minimum in the centre where the density of wavefields is small and increases very sharply at the edges where the density of wavefields is large, although it is the reverse for the reflecting power I_{hj}. This effect, called the *margin effect*, was predicted qualitatively by Borrmann (1959) and von Laue (1960), demonstrated experimentally by Kato & Lang (1959), and calculated by Kato (1960).

(ii) Large values of $\mu_o t$ (of the order of 6 or more) (Fig. 5.1.8.3*b*). The predominant factor is now anomalous absorption. The wavefields propagating along the edges of the Borrmann triangle undergo normal absorption, while those propagating parallel to the lattice planes (or nearly parallel) correspond to tie points in the centre of the dispersion surface and undergo anomalously low absorption. The intensity distribution now has a maximum in the centre. For values of μt larger than 10 or so, practically only the wavefields propagating parallel to the lattice planes go through the crystal, which acts as a wave guide: this is the Borrmann effect.

5.1.8.3. Spherical-wave Pendellösung

Fig. 5.1.8.4 shows that along any path Ap inside the Borrmann triangle two wavefields propagate, one with tie point P_1, on branch 1, the other with the point P'_2, on branch 2. These two points lie on the extremities of a diameter of the dispersion surface. The two wavefields interfere, giving rise to *Pendellösung* fringes, which were first observed by Kato & Lang (1959), and calculated by Kato (1961*b*). These fringes are of course quite different from the plane-wave *Pendellösung* fringes predicted by Ewald (Section 5.1.6.3) because the tie points of the interfering wavefields are different and their period is also different, but they have in common the fact that they result from interference

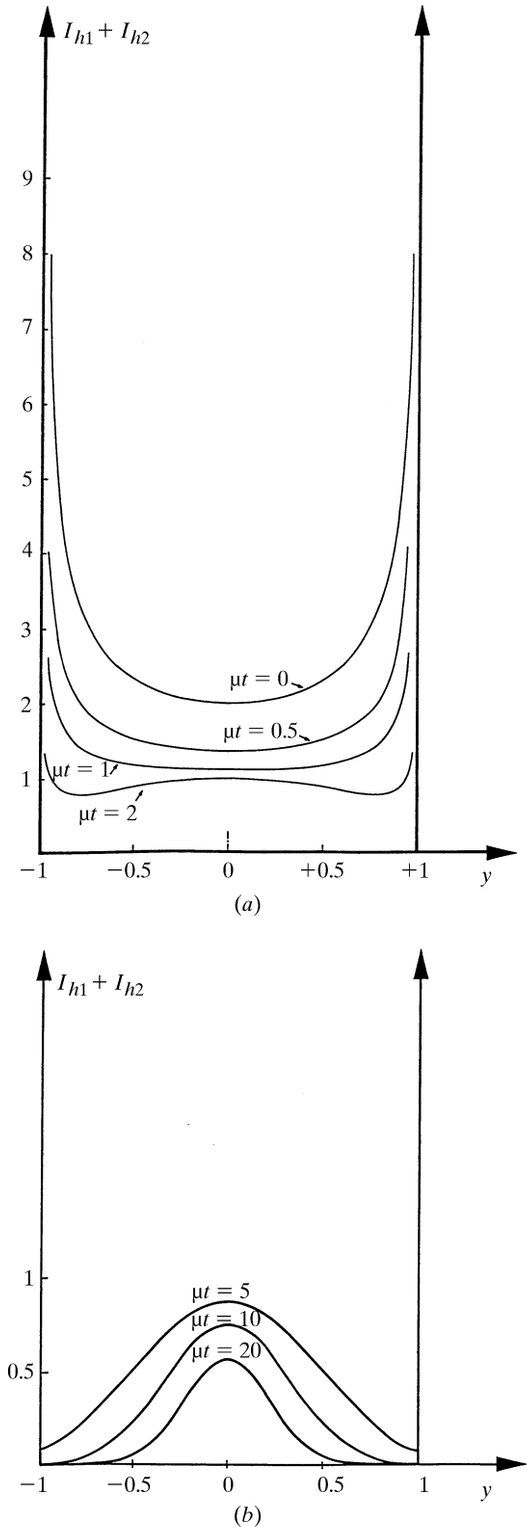

Fig. 5.1.8.3. Intensity distribution along the base of the Borrmann triangle. y is a normalized coordinate along BC. (*a*) Small values of μt. The interference (spherical-wave *Pendellösung*) between branch 1 and branch 2 is neglected. (*b*) Large values of μt.

between wavefields belonging to different branches of the dispersion surface.

Kato has shown that the intensity distribution at any point at the base of the Borrmann triangle is proportional to

$$\left\{J_o\left[A(x_o x_h)^{1/2}\right]\right\}^2,$$

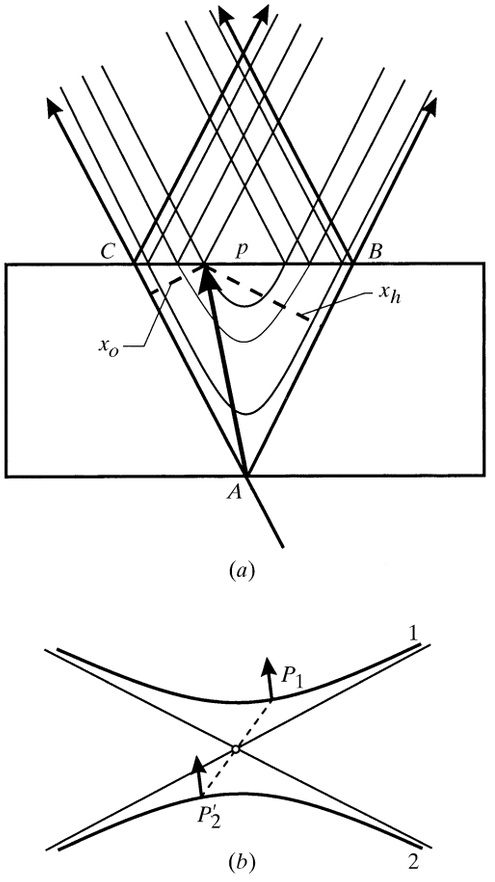

Fig. 5.1.8.4. Interference at the origin of the *Pendellösung* fringes in the case of an incident spherical wave. (*a*) Direct space; (*b*) reciprocal space.

where $A = 2\pi(\gamma_o\gamma_h)^{1/2}/(\Lambda_L \sin\theta)$ and x_o and x_h are the distances of p from the sides AB and AC of the Borrmann triangle (Fig. 5.1.8.4). The equal-intensity fringes are therefore located along the locus of the points in the triangle for which the product of the distances to the sides is constant, that is hyperbolas having AB and AC as asymptotes (Fig. 5.1.8.4*b*). These fringes can be observed on a section topograph of a wedge-shaped crystal (Fig. 5.1.8.5). The technique of section topography is described in *IT* C, Section 2.7.2.2. The *Pendellösung* distance Λ_L depends on the polarization state [see equation (5.1.3.8)]. If the incident wave is unpolarized, one observes the superposition of the *Pendellösung* fringes corresponding to the two states of polarization, parallel and perpendicular to the plane of incidence. This results in a beat effect, which is clearly visible in Fig. 5.1.8.5.

APPENDIX A5.1.1
Basic equations

A5.1.1.1. Dielectric susceptibility – classical derivation

Under the influence of the incident electromagnetic radiation, the medium becomes polarized. The dielectric susceptibility, which relates this polarization to the electric field, thus characterizes the interaction of the medium and the electromagnetic wave. The classical derivation of the dielectric susceptibility, χ, which is summarized here is only valid for a very high frequency which is also far from an absorption edge. Let us consider an electromagnetic wave,

$$\mathbf{E} = \mathbf{E_o} \exp 2\pi i(\nu t - \mathbf{k}\cdot\mathbf{r}),$$

references